Scaling properties of the action in the Riemann-Liouville fractional standard map

J. A. Méndez-Bermúdez
Instituto de Física, Benemérita Universidad Autónoma de Puebla, Puebla 72570, Mexico

R. Aguilar-Sánchez
Facultad de Ciencias Químicas, Benemérita Universidad Autónoma de Puebla, Puebla 72570, Mexico

José M. Sigarreta
Facultad de Matemáticas, Universidad Autónoma de Guerrero, Carlos E. Adame No. 54 Col. Garita, Acalpulco Gro. 39650, Mexico

Edson D. Leonel
Universidade Estadual Paulista (UNESP), Departamento de Física, Av. 24A, 1515, Bela Vista, CEP: 13506-900 Rio Claro, SP, Brazil

(Received 14 December 2023; accepted 29 February 2024; published 29 March 2024)

The Riemann-Liouville fractional standard map (RL-fSM) is a two-dimensional nonlinear map with memory given in action-angle variables (I, θ). The RL-fSM is parameterized by K and $\alpha \in (1, 2]$, which control the strength of nonlinearity and the fractional order of the Riemann-Liouville derivative, respectively. In this work we present a scaling study of the average squared action $\langle I^2 \rangle$ of the RL-fSM along strongly chaotic orbits, i.e., for $K \gg 1$. We observe two scenarios depending on the initial action I_0, $I_0 \ll K$ or $I_0 \gg K$. However, we can show that $\langle I^2 \rangle / I_0^2$ is a universal function of the scaled discrete time nK^2/I_0^2 (n being the nth iteration of the RL-fSM). In addition, we note that $\langle I^2 \rangle$ is independent of α for $K \gg 1$. Analytical estimations support our numerical results.

DOI: 10.1103/PhysRevE.109.034214

I. PRELIMINARIES

The kicked rotor represents a free rotating stick in an inhomogeneous field that is periodically switched on in instantaneous pulses; see, e.g., Ref. [1]. It is described by the second-order differential equation

$$\ddot{\theta} + K \sin(\theta) \sum_{j=0}^{\infty} \delta\left(\frac{t}{T} - j\right) = 0. \qquad (1)$$

Here, $\theta \in [0, 2\pi]$ is the angular position of the stick, K is the kicking strength, T is the kicking period (that we set to one from now on), and δ is Dirac δ function. By replacing the second-order derivative in the equation of motion of the kicked rotor with a Riemann-Liouville (RL) derivative of fractional order α [2,3], the RL fractional kicked rotor (fKR) is obtained [4,5]:

$${}_0D_t^{\alpha}\theta + K \sin(\theta) \sum_{j=0}^{\infty} \delta(t - j) = 0, \quad 1 < \alpha \leqslant 2. \qquad (2)$$

Above [2,3],

$$\begin{aligned} {}_0D_t^{\alpha}\theta(t) &= D_t^m {}_0\mathcal{I}_t^{m-\alpha}\theta(t) \\ &= \frac{1}{\Gamma(m-\alpha)} \frac{d^m}{dt^m} \int_0^t \frac{\theta^{\tau} d\tau}{(t-\tau)^{\alpha-m+1}}, \end{aligned}$$
$$m - 1 < \alpha \leqslant m,$$

with $D_t^m = d^m/dt^m$, ${}_0\mathcal{I}_t^m f(t)$ is a fractional integral given by

$${}_0\mathcal{I}_t^m f(t) = \frac{1}{\Gamma(m)} \int_0^t (t-\tau)^{\alpha-1} f(\tau) d\tau,$$

and Γ is the Gamma function.

The RL-fKR has a stroboscopic version, a two-dimensional nonlinear map with memory, which is well known as the RL fractional standard map (RL-fSM) [5]:

$$\begin{aligned} I_{n+1} &= I_n - K \sin(\theta_n), \\ \theta_{n+1} &= \frac{1}{\Gamma(\alpha)} \sum_{i=0}^{n} I_{i+1} V_{\alpha}^1(n - i + 1), \quad \mod(2\pi), \end{aligned} \qquad (3)$$

where $I(t) \equiv {}_0D_t^{\alpha-1}\theta(t)$, n is the discrete time, and $V_{\alpha}^k(m) = m^{\alpha-k} - (m-1)^{\alpha-k}$. Then, the RL-fSM, given in action-angle variables (I, θ), is parameterized by K and $\alpha \in (1, 2]$, which control the strength of nonlinearity and the fractional order of the RL derivative, respectively. In fact, for $\alpha = 2$, the RL-fSM reproduces the celebrated Chirikov standard map (CSM) [6].

Compared with the CSM, which presents the generic transition to chaos (in the context of the Kolmogorov-Arnold-Moser theorem), depending on the parameter pair (K, α), the RL-fSM shows richer dynamics: It generates attractors (fixed points, asymptotically stable periodic trajectories, slow converging and slow diverging trajectories, ballistic trajectories, and fractal-like structures) and/or chaotic trajectories [5,7–10]. Moreover, trajectories may intersect, and attractors may overlap [7].

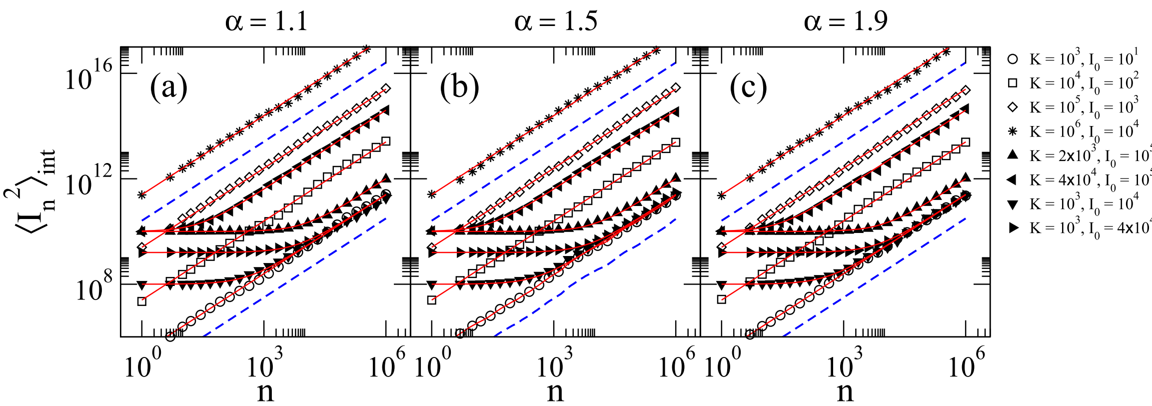

FIG. 1. Average squared action $\langle I_n^2\rangle_{\rm int}$ as a function of the discrete time n for (a) $\alpha = 1.1$, (b) $\alpha = 1.5$, and (c) $\alpha = 1.9$. Open symbols (full symbols) correspond to $I_0 \ll K$ ($I_0 \gg K$). The blue dashed lines, plotted to guide the eye, are proportional to n. The average is over 100 orbits with initial random phases in the interval $0 < \theta_0 < 2\pi$. Red full lines are Eq. (9).

Among the available studies on the RL-fKR, e.g., Refs. [5,7–10], the analysis of strongly chaotic orbits has been left unexplored. Therefore, here we undertake this task and characterize the dynamics of the RL-fSM by computing the squared average action $\langle I_n^2\rangle$ when $K \gg 1$.

II. NUMERICAL RESULTS

For the numerical study we wrote a program in FORTRAN90 to compute the orbits of map (3) by straightforward iteration. Moreover, since the memory property in map (3) forbids the use of a large number of orbit realizations, instead of investigating $\langle I_n^2\rangle$ directly, to smooth the curves $\langle I_n^2\rangle$ vs n, we compute its cumulative-normalized value:

$$\langle I_n^2\rangle_{\rm int} = \frac{1}{n}\int_{n_0=0}^{n}\langle I_{n'}^2\rangle dn'. \tag{4}$$

Specifically, we compute $\langle I_n^2\rangle_{\rm int}$ for map (3) following two steps: First we calculate the average squared action over the orbit associated with the initial condition j as $\langle I_{n,j}^2\rangle = (n+1)^{-1}\sum_{i=0}^{n} I_{i,j}^2$, where i refers to the ith iteration of the map. Then, $\langle I_n^2\rangle_{\rm int}$ is defined as the average over $M = 100$ independent realizations of the map (by randomly choosing values of θ_0 in the interval $0 < \theta_0 < 2\pi$): $\langle I_n^2\rangle_{\rm int}(I_0, K, \alpha) = M^{-1}\sum_{j=1}^{M}\langle I_{n,j}^2\rangle$.

In Fig. 1 we plot $\langle I_n^2\rangle_{\rm int}$ as a function of the discrete time n for representative values of α in the interval (1,2]: (a) $\alpha = 1.1$, (b) $\alpha = 1.5$, and (c) $\alpha = 1.9$. Several combinations of parameter pairs (I_0, K) are considered, as indicated in the right-hand side of the figure. From this figure we observe two scenarios, depending on the initial action I_0 as compared with K: $I_0 \ll K$ (open symbols) or $I_0 \gg K$ (full symbols). Specifically, when $I_0 \ll K$, $\langle I_n^2\rangle_{\rm int} \propto n$ for all n (see the blue dashed lines), while for $I_0 \gg K$, first, $\langle I_n^2\rangle_{\rm int}$ remains approximately constant and proportional to I_0^2 up to a crossover time n^*, after which $\langle I_n^2\rangle_{\rm int}$ grows proportional to n.

From Fig. 1 it can also be seen that the crossover time n^* depends on both I_0 and K, while the dependence of n^* with α is not evident. Then, to look for the dependence of n^* on the map parameters, in Fig. 2(a) [Fig. 2(b)] we plot $\langle I_n^2\rangle_{\rm int}$ vs n for several values of I_0 [K] and fixed K [I_0]. In both figures we use $\alpha = 1.1$. We numerically extract n^* as the crossing point between the functions $\langle I_n^2\rangle_{\rm int} = I_0^2$ and $\langle I_n^2\rangle_{\rm int} = \mathcal{C}n$ (which is the fitting to the data in the growing regime); as examples,

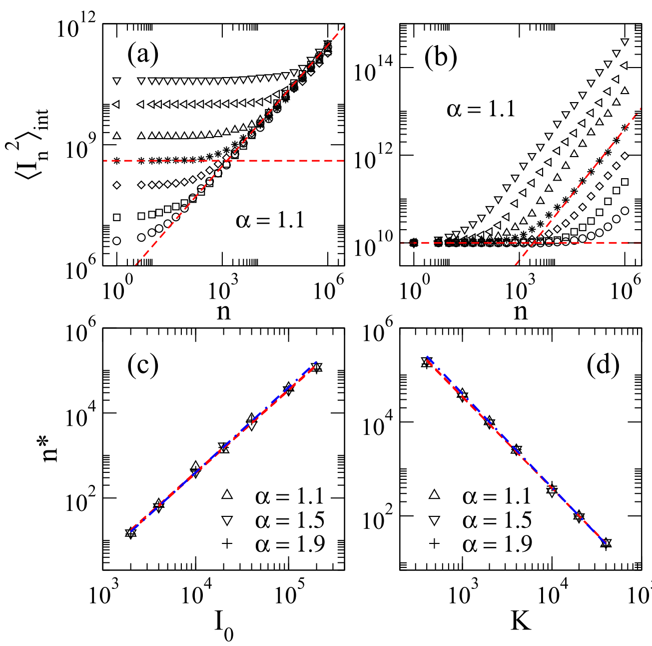

FIG. 2. (a), (b) Average squared action $\langle I_n^2\rangle_{\rm int}$ as a function of n for (a) $K = 10^3$ and several values of I_0 (2×10^3, 4×10^3, 10^4, 2×10^4, 4×10^4, 10^5, and 2×10^5, from bottom to top) and (b) $I_0 = 10^5$ and several values of K (4×10^2, 10^3, 2×10^3, 4×10^3, 10^4, 2×10^4, and 4×10^4, from bottom to top). As in Fig. 1, the average is taken over 100 orbits with initial random phases in the interval $0 < \theta_0 < 2\pi$. All data in (a), (b) correspond to $\alpha = 1.1$. The horizontal red dashed lines in (a), (b) indicate $\langle I_n^2\rangle_{\rm int} = I_0^2$ with (a) $I_0 = 4\times10^4$ and (b) $I_0 = 10^5$, respectively. The transverse red dashed lines in (a), (b) are fittings of $\langle I_n^2\rangle_{\rm int} = \mathcal{C}n$ to the data represented by asterisks (for $n \geqslant 10^4$) with fitting constants (a) $\mathcal{C} = 294\,658$ and (b) $\mathcal{C} = 3\,984\,348$. (c), (d) Crossover time n^* (c) as a function of I_0 for constant K ($K = 10^3$) and (d) as a function of K for constant I_0 ($I_0 = 10^5$). In (c), (d), three values of α are reported: $\alpha = 1.1$, 1.5, and 1.9. Red dashed lines in (c), (d) are power-law fittings to the data of the form (a) $n^* \propto I_0^{\gamma_1}$ with $\gamma_1 \approx 2$ and (b) $n^* \propto K^{\gamma_2}$ with $\gamma_2 \approx -2$. Blue dot-dashed lines in (c), (d) are Eq. (11).

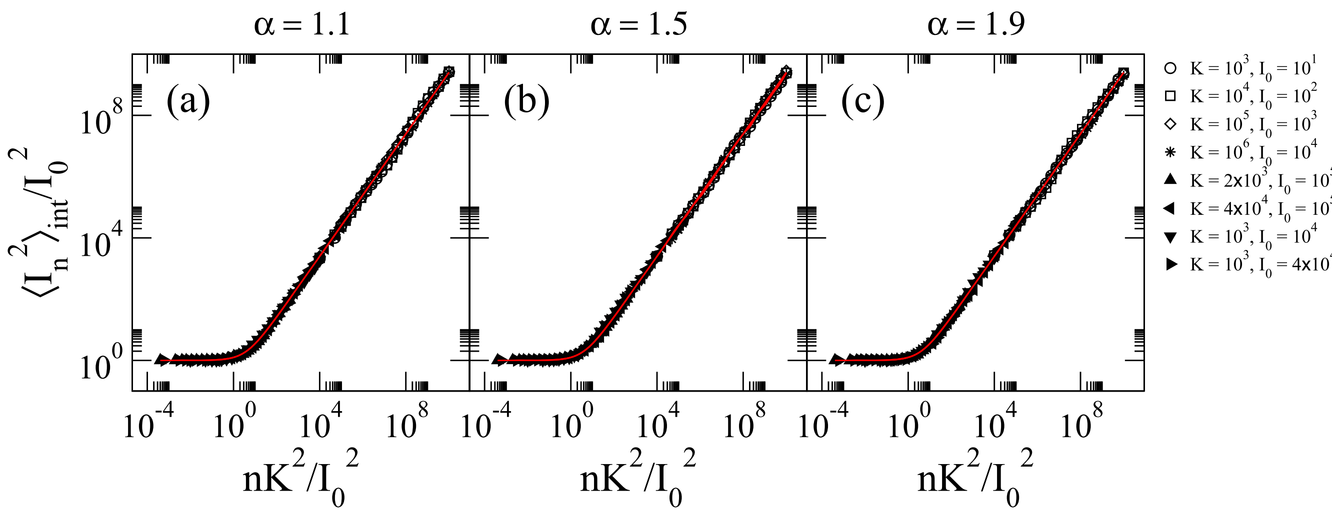

FIG. 3. Normalized average squared action $\langle I_n^2\rangle_{\rm int}/I_0^2$ as a function of the normalized time nK^2/I_0^2. Same data sets as in Fig. 1. The red line is Eq. (10).

see the horizontal and transverse dashed lines in Figs. 2(a) and 2(b), respectively. Thus, in Figs. 2(c) and 2(d) we plot the obtained values of n^* for $\alpha = 1.1$ but also for $\alpha = 1.5$ and 1.9. Figures 2(c) and 2(d) reveal the power-law dependence

$$n^* \propto I_0^{\gamma_1} K^{\gamma_2} \tag{5}$$

and the independence of n^* on α. Power-law fittings of the data in Figs. 2(c) and 2(d) provide $\gamma_1 \approx 2$ and $\gamma_2 \approx -2$, see red dashed lines.

Equation (5) together with the observation that $\langle I_n^2\rangle_{\rm int} \approx I_0^2$ for $n < n^*$ allow us to scale the curves $\langle I_n^2\rangle_{\rm int}$ vs n. Indeed, in Fig. 3 we plot $\langle I_n^2\rangle_{\rm int}/I_0^2$ as a function of the normalized time nK^2/I_0^2 (i.e., n/n^*) and observe the collapse of all curves on top of a *universal* function.

III. ANALYTICAL ESTIMATION

Now, to support and better understand the scaling performed above, we derive an analytical estimation for $\langle I_n^2\rangle_{\rm int}$; see, e.g., Ref. [11]. From the first line of map (3) we have that $I_{n+1}^2 = I_n^2 - 2KI_n\sin(\theta_n) + K^2\sin^2(\theta_n)$, so we can write

$$\langle I_{n+1}^2\rangle = \langle I_n^2\rangle - 2K\langle I_n\rangle\langle\sin(\theta_n)\rangle + K^2\langle\sin^2(\theta_n)\rangle.$$

Since for chaotic orbits we can assume that $\langle\sin(\theta_n)\rangle = 0$, the term $2K\langle I_n\rangle\langle\sin(\theta_n)\rangle$ can be eliminated. Therefore

$$\langle I_{n+1}^2\rangle = \langle I_n^2\rangle + \frac{K^2}{2}, \tag{6}$$

where we have used $\langle\sin^2(\theta_n)\rangle = 1/2$. Then, by noticing that

$$\langle I_{n+1}^2\rangle - \langle I_n^2\rangle = \frac{\langle I_{n+1}^2\rangle - \langle I_n^2\rangle}{(n+1)-n} \approx \frac{dJ}{dn},$$

we rewrite Eq. (6) as the first-order differential equation,

$$\frac{dJ}{dn} = \frac{K^2}{2}, \tag{7}$$

where $J \equiv \langle I_n^2\rangle$. Therefore, by solving (7) we can write

$$\langle I_n^2\rangle = I_0^2 + \frac{K^2}{2}n, \tag{8}$$

where we have used $J_0 = \langle I_0^2\rangle = I_0^2$ and $n_0 = 0$. Finally, by substituting Eq. (8) into Eq. (4), we can also write down an explicit expression for $\langle I_n^2\rangle_{\rm int}$:

$$\langle I_n^2\rangle_{\rm int} = I_0^2 + \frac{K^2}{4}n. \tag{9}$$

Indeed, Eq. (9) reproduces our numerical data well, as can be seen in Fig. 1 where we have included Eq. (9) as red lines.

IV. DISCUSSION AND CONCLUSIONS

Given the good correspondence of Eq. (9) and the numerical data, it is clear that it reproduces the scaling laws reported in Sec. II, which can be summarized as

$$\langle I_n^2\rangle_{\rm int} = \begin{cases} \propto K^2 n\,, & \text{when} \quad I_0 \ll K, \\ \left.\begin{matrix} \approx I_0^2\,, & n < n^* \\ \propto K^2 n\,, & n > n^* \end{matrix}\right\} & \text{when} \quad I_0 \gg K. \end{cases}$$

Moreover, Eq. (9) can also be used to demonstrate that the ratio $\langle I_n^2\rangle_{\rm int}/I_0^2$ is a simple *universal* function of the variable $\overline{n} = n/n^*$:

$$\frac{\langle I_n^2\rangle_{\rm int}}{I_0^2} = 1 + \overline{n}, \tag{10}$$

where the crossover time n^* is now naturally defined as

$$n^* \equiv 4I_0^2K^{-2}, \tag{11}$$

in agreement with Eq. (5). Finally, in Figs. 2(c) and 2(d), and 3 we plot Eqs. (11) and (10) (see dot-dashed blue lines and red full lines), respectively, and observe an excellent agreement with the numerical data.

It is relevant to notice that for strongly chaotic orbits, $K \gg 1$, the average squared action $\langle I_n^2\rangle$ for the RL-fSM does not depend on the order α of the fractional derivative. Indeed, the panorama reported here for $\langle I_n^2 \rangle$ vs n is equivalent to that of CSM [11,12] as well as that of the discontinuous standard map [11,13], both with $K \gg 1$. This could be understood from the analytical estimation of Sec. III by noticing that to obtain the expression for $\langle I_n^2 \rangle$ we mainly used the first equation of map (3), which does not contain the parameter α; i.e., the property of memory, parametrized by α, is only present in the equation for θ, which is a cyclic variable. So when $K \gg 1$, $\langle I_n^2 \rangle$ must be independent of α. That is, to observe effects of α on the dynamics of the RL-fSM, $K \sim 1$ should be set, see Refs. [5,7–10].

We stress that similar studies can be carried out for other types of nonlinearity (not just the continuous sine-shaped nonlinearity in the first equation of the RL-fSM) and for other types of fractional derivatives. This, in fact, will be the subject of future investigations.

Finally, we want to add that our work falls within the scope of the general fractional dynamics (GFDynamics), a line of research recently introduced in Ref. [14].

ACKNOWLEDGMENTS

J.A.M.-B. expresses thanks for support from CONAHCyT-Fronteras (Grant No. 425854) and VIEP-BUAP (Grant No. 100405811-VIEP2024), Mexico. The research of J.M.S. is supported by a grant from Agencia Estatal de Investigación (PID2019-106433GB-I00/AEI/10.13039/501100011033), Spain. E.D.L. acknowledges support from CNPq (No. 301318/2019-0) and FAPESP (No. 2019/14038-6), Brazil.

[1] E. Ott, *Chaos in Dynamical Systems* (Cambridge University Press, Cambridge, England, 2008).
[2] S. G. Samko, A. A. Kilbas, and O. I. Marichev, *Fractional Integrals and Derivatives, Theory and Applications* (Gordon and Breach, New York, 1993).
[3] A. A. Kilbas, H. M. Srivastava, and J. J. Trujillo, *Theory and Application of Fractional Differential Equations* (Elsevier, Amsterdam, 2006).
[4] V. E. Tarasov and G. M. Zaslavsky, Fractional equations of kicked systems and discrete maps, J. Phys. A: Math. Theor. **41**, 435101 (2008).
[5] M. Edelman and V. E. Tarasov, Fractional standard map, Phys. Lett. A **374**, 279 (2009).
[6] B. V. Chirikov, Research concerning the theory of nonlinear resonance and stochasticity, Preprint 267, Institute of Nuclear Physics, Novosibirsk (1969) [Engl. Trans. CERN Trans. 71-40 (1971)].
[7] M. Edelman, Fractional standard map: Riemann-Liouville vs. Caputo, Commun. Nonlinear Sci. Numer. Simul. **16**, 4573 (2011).
[8] M. Edelman and L. A. Taieb, New types of solutions of non-linear fractional differential equations, in *Advances in Harmonic Analysis and Operator Theory*, edited by A. Almeida, L. Castro, and F.-O. Speck, Operator Theory: Advances and Applications Series (Springer, Basel, 2013), pp. 139–155.
[9] M. Edelman, Dynamics of nonlinear systems with power-law memory, in *Handbook of Fractional Calculus with Applications*, edited by V. E. Tarasov, Applications in Physics Vol. 4, Part A (De Gruyter, Berlin, Boston, 2019), pp. 103–132.
[10] J. A. Mendez-Bermudez, K. Peralta-Martinez, J. M. Sigarreta, and E. D. Leonel, Leaking from the phase space of the Riemann-Liouville fractional standard map, Chaos, Solitons Fractals **172**, 113532 (2023).
[11] J. A. Mendez-Bermudez, J. A. de Oliveira, and E. D. Leonel, Analytical description of critical dynamics for two-dimensional dissipative nonlinear maps, Phys. Lett. A **380**, 1959 (2016).
[12] D. G. Ladeira and J. K. L. da Silva, Scaling properties of a simplified bouncer model and of Chirikov's standard map, J. Phys. A: Math. Theor. **40**, 11467 (2007).
[13] J. A. Mendez-Bermudez and R. Aguilar-Sanchez, Scaling properties of discontinuous maps, Phys. Rev. E **85**, 056212 (2012).
[14] V. E. Tarasov, General fractional dynamics, Mathematics **9**, 1464 (2021).